THE JOURNAL OF IMMUNOLOGY

Autotaxin through Lysophosphatidic Acid Stimulates Polarization, Motility, and Transendothelial Migration of Naive T Cells

Yafeng Zhang, Yi-Chun Maria Chen, Matthew F. Krummel and Steven D. Rosen

J Immunol published online 7 September 2012
http://www.jimmunol.org/content/early/2012/09/07/jimmunol.1201604

The Journal of Immunology is published twice each month by The American Association of Immunologists, Inc., 9650 Rockville Pike, Bethesda, MD 20814-3994.

Print ISSN: 0022-1767 Online ISSN: 1550-6606.

Published September 7, 2012, doi:10.4049/jimmunol.1201604

Autotaxin through Lysophosphatidic Acid Stimulates Polarization, Motility, and Transendothelial Migration of Naive T Cells

Yafeng Zhang,*,† Yi-Chun Maria Chen,†,‡ Matthew F. Krummel,†,‡ and Steven D. Rosen*,†

Blood-borne lymphocytes home to lymph nodes by interacting with and crossing high endothelial venules (HEVs). The transendothelial migration (TEM) step is poorly understood. Autotaxin (ATX) is an ectoenzyme that catalyzes the conversion of lysophosphatidylcholine (LPC) to lysophosphatidic acid (LPA), a bioactive lipid and a close relative of sphingosine 1-phosphate. HEVs produce and secrete ATX into the blood. A prior study implicated ATX in the overall homing process, but the step in which it functions and its mechanism of action have not been defined. In this article, we show that HA130, an inhibitor of the enzymatic activity of ATX, slows T cell migration across lymph node HEVs in vivo. Ex vivo, ATX plus LPC or LPA itself induces the polarization of mouse naive T cells and stimulates their motility on an ICAM-1 substratum. Under physiologic shear conditions in a flow chamber, LPA or ATX/LPC strongly enhances TEM of integrin-arrested T cells across an endothelial monolayer. HA130 blunts the TEM-promoting activity of ATX, paralleling its in vivo effects. T cells possess Mn^{+2}-activatable receptors for ATX, which are localized at the leading edge of polarized cells. ATX must bind to these receptors to elicit a maximal TEM response, providing a mechanism to focus the action of LPA onto arrested lymphocytes in flowing blood. Our results indicate that LPA produced via ATX facilitates T cell entry into lymph nodes by stimulating TEM, substantiating an additional step in the homing cascade. This entry role for LPA complements the efflux function of sphingosine 1-phosphate. ***The Journal of Immunology*****, 2012, 189: 000–000.**

Lymphocyte migration (homing) from the blood into secondary lymphoid organs (SLOs) is an essential step in lymphocyte recirculation, the process by which the repertoire of naive lymphocytes rapidly cycles through SLOs, thereby enabling contact between sequestered Ags and rare cognate lymphocytes (1–3). For all SLOs except spleen, the portal of entry for blood-borne lymphocytes is high endothelial venules (HEVs) (1, 4, 5). These vessels are functionally specialized to capture lymphocytes from the flowing blood and to support their migration into SLOs. As is generally the case for leukocyte–endothelial cell (EC) interactions (6), naive T cell recruitment across HEVs occurs in several sequential steps: rolling of lymphocytes along the endothelium, arrest on the endothelium, intraluminal crawling, and finally transendothelial migration (TEM) into the SLO (2, 4, 5). In peripheral lymph node (PLN) HEVs, the first step is mediated by transient interactions between L-selectin on lymphocytes and a complex of mucins on HEVs (7). The second step is due to arrest chemokines, such as CCL21, which are immobilized apically on HEVs (2, 5, 8). Signaling through CCR7, CCL21 activates αLβ2 on lymphocytes, which increases the integrin's affinity for ICAM-1/ICAM-2 on HEVs, leading to the rapid arrest of the rolling cells (8–10). Some of the lymphocytes crawl intraluminally for several minutes before undergoing TEM, whereas the remainder undergo TEM without migration (11). TEM occurs within 2.5 min for T cells (11). Shear stress provided by blood flow is required for both the integrin-mediated arrest and TEM steps (12, 13).

Previously, gene profiling of purified HEV-ECs unexpectedly revealed a very high expression of autotaxin (ATX) transcripts (14). ATX was initially discovered as a secreted protein from A2058 melanoma cells, which enhances their own motility (15). ATX is an ∼110-kDa protein with two N-terminal somatomedin B-like domains, a phosphodiesterase domain, and a C-terminal nuclease-like domain (16, 17). ATX was later shown to be a lysophospholipase D, which catalyzes the conversion of lysophosphatidylcholine (LPC) to lysophosphatidic acid (LPA) (18). As an extracellular lysophospholipid, LPA engages six GPCRs (termed LPA1–6) and evokes diverse growth factor-like responses (motility, proliferation, survival, and differentiation) in multiple cell types (19, 20). LPA is now known to be responsible for the motility-promoting action of ATX on A2058 cells, as well as on other cancer and normal cells (21). ATX performs essential functions in vasculogenesis and neural tube formation during embryonic development (22, 23). In the adult, ATX is present in the blood and is responsible for the maintenance of LPA in plasma (22, 23). In mice, the normal level of LPA is 200–400 nM (24), and in humans it is 80–90 nM (25). Pathologic roles for ATX are indicated in cancer and cardiovascular disease (26, 27). In the context of immune function, ATX is overexpressed in synovial fibroblasts in rheumatoid arthritis and has been implicated in the pathogenic process (28). LPA acting through LPA2 inhibits dendritic cell activation and dampens allergic airway inflammation (29).

*Department of Anatomy, University of California San Francisco, San Francisco, CA 94143; †Program in Immunology, University of California San Francisco, San Francisco, CA 94143; and ‡Department of Pathology, University of California San Francisco, San Francisco, CA 94143

Received for publication June 11, 2012. Accepted for publication August 14, 2012.

This work was supported by grants from the National Institutes of Health (R01-GM57411 and R01-GM23547 to S.D.R. and AI52116 to M.F.K.). Y.Z. was supported by a postdoctoral fellowship from the American Heart Association (A115033).

Address correspondence and reprint requests to Dr. Steven Rosen, University of California San Francisco, 513 Parnassus Avenue, Box 0452, San Francisco, CA 94143. E-mail address: steven.rosen@ucsf.edu

The online version of this article contains supplemental material.

Abbreviations used in this article: ATX, autotaxin; b-ATX, biotin linked to autotaxin; EC, endothelial cell; HEV, high endothelial venule; LN, lymph node; LPA, lysophosphatidic acid; LPAR, lysophosphatidic acid receptor; LPC, lysophosphatidylcholine; MLN, mesenteric lymph node; PLN, peripheral lymph node; PTX, pertussis toxin; SLO, secondary lymphoid organ; S1P, sphingosine 1-phosphate; TEM, transendothelial migration.

The discovery of abundant ATX transcripts in HEV-ECs prompted two studies, which confirmed that ATX protein is expressed in HEVs of SLOs (30, 31). We further found that ATX is secreted apically by HEV-ECs; ATX can bind to receptors on chemokine-activated T cells; LPA is chemokinetic for T cells; and injection of a catalytically inactive form of ATX (T210A) partially inhibits homing of T cells into SLOs (30). These findings led to a paracrine model of ATX function in homing (30), whereby ATX is secreted into the lumens of HEVs and binds to proximally arrested T cells. The bound ATX uses the abundant LPC in the plasma (~200 μM) to produce LPA, which promotes T cell entry into the lymphoid organ.

This speculative model has awaited further in vivo validation and a mechanistic understanding of how ATX and its enzymatic product LPA influence lymphocyte migration upon and across an endothelial substratum under physiologic shear stress conditions. The present study addresses these issues.

Materials and Methods

Reagents

Mouse ICAM-1–Fc (796-IC-050), CCL21 (457-6C-025), and TNF-α (210-TA) were from R&D Systems (Minneapolis, MN). The Abs used were anti-CD44 (IM7; BD Biosciences, San Jose, CA), anti-CD3e (45-2C11; BD), anti-B220 (RA3-6B2; BD), anti-autotaxin AF5255; R&D Systems), anti-CD49d (PS/2; Serotec, Raleigh, NC), and anti-CD43 (eBioR2/60; eBiosciences, San Diego, CA). Stock solutions of LPA (18:1 Oleoyl-LPA; L7260, Sigma-Aldrich, St. Louis, MO) were made in methanol (10 mM) and stored at −80°C. Dilutions into aqueous buffers were prepared just before use, with methanol serving as the carrier control. We used 18:1 LPA for our studies because it occurs naturally in blood (24) and is one of the enzymatic products of ATX (32). Fatty-acid free BSA (A8806), L-α-lysophosphatidylcholine (L4129), pertussis toxin (PTX), and Y-27632 were from Sigma-Aldrich. BrP-LPA was from Echelon (Logan, UT). The biotinylation-labeling kit (704-0030) came from Novus (St. Charles, MO). Cy2-streptavidin (016-220-084) and Cy3–anti-rat IgG (712-166-150) were from Jackson ImmunoResearch (West Grove, PA).

Mice

All mouse protocols were approved by the University of California San Francisco Committee for Animal Research. C57BL/6 female mice (6–8 wk; Charles River Labs, Wilmington, MA) were used for homing assays. OTII, Ub-GFP, *Itgb2* null, and *Itgb3* null mice were from The Jackson Laboratory. OTII-GFP mice were obtained by crossing OTII mice with Ub-GFP mice.

Cells

$CD3^+$ T cells were purified from mechanically dispersed PLNs using the EasySep T cell Enrichment Kit (StemCell Tech, Vancouver, BC, Canada). For motility assays, $CD4^+$ T cells were purified from PLNs of OTII Ub-GFP mice using the EasySep Mouse $CD4^+$ T Cell Enrichment Kit (StemCell Tech). Purified cells were resuspended in RPMI 1640 plus 10% charcoal-dextran–treated FBS and incubated at 37°C for ~1 h before imaging. At least 90% of the $CD3^+$ cells and ≥95% of the $CD4^+$ T cells were naive, as defined by the criterion of $CD44^{lo}$. For most of the experiments, these populations are referred to as naive T cells. TK1 cells were maintained in RPMI 1640 with 10% FBS, 100 U/ml penicillin, 100 μg/ml streptomycin, and 25 μM 2-ME.

T cell homing

Short-term homing of T cells was carried out as described (30). CFSE-labeled $CD3^+$ T cells (20×10^6 in 100 μl), with or without HA130 (2 nmol/g recipient mouse), in DMSO were injected i.v. into mice. HA130 or DMSO was reinjected at 7 and 12 min. At 15 min, SLOs were cryostat processed for immunohistochemistry to highlight HEVs (MECA-79 staining for lymph nodes and CD31 staining for Peyer's patches). The number of fluorescent lymphocytes outside HEVs (in the lymphoid organ parenchyma) and within HEVs (both in the lumens and walls) were counted. Two mice were processed at a time (one HA130 and one control). Six nonconsecutive sections from two mesenteric lymph nodes (MLNs) and three PLNs of each mouse were evaluated. Ratios were determined for each section, and a mean ratio was computed for each mouse. Means from three mice/group were combined to yield overall means ± SDs.

ATX/T210A preparation

The recombinant proteins were prepared as described previously (30).

Uropod assay

Eight-well chamber slides (154534, Lab-Tek; Thermo, Rochester, NY) were coated with 3 μg/ml ICAM-1–Fc and CCL21 overnight. The slides were then blocked with 3% fatty acid-free BSA for 1 h. TK1 lymphoma cells were cultured with 5% charcoal-dextran–treated FBS overnight; $CD3^+$ T cells were cultured with 10% charcoal-dextran–treated FBS for 2 h. Cells ($0.5–1 \times 10^6$) were added to the chamber (200 μl) containing HBSS buffer with 0.2% fatty acid-free BSA. LPA or ATX/LPC were added, and cells were allowed to settle at 37°C. Attached cells were fixed with 4% formaldehyde in PBS. After washing and blocking with BSA, uropods were visualized by staining with anti-CD44 or CD43 in combination with secondary Abs. For Gαi or ROCK inhibition, cells were cultured for 2 h with PTX (200 ng/ml) or Y27632 (10 μM), respectively. For ATX-inhibition experiments, cells were incubated with HA130 (0.3 μM) or BrP-LPA (10 μM) for 30 min prior to the addition of ATX.

Cell-motility assays

Custom crawling chambers were assembled. Dividers for six chambers were made from polydimethylsiloxane (SYLGARD 184 Silicone Elastomer Kit, 10:1 mix; Midland, MI) formed in a printed mold. Each divider was cut out using a scalpel, placed on top of a glass slide (48311-703; VWR, Batavia, IL), and covered with a No.1 cover glass (48393-059; VWR) to create the chambers. For assays, the chambers were freshly coated with 3 μg/ml ICAM-1/Fc, with or without 400 ng/ml CCL21, at 4°C overnight. The chambers were washed in PBS, blocked with PBS plus 0.5% fatty acid-free BSA, and kept in the blocking buffer until use. A total of 5×10^4 OTII Ub-GFP $CD4^+$ T cells was resuspended in 100 μl block and seeded into the chamber. For LPA treatment, 1 μM LPA was added to the cells immediately before imaging. For ATX/LPC treatment, cells were incubated with 1 μg/ml ATX for 5 min, followed by 10 μM LPC cells immediately before imaging. Imaging was done with a Zeiss Axiovert 200M microscope with a Plan-Neofluar 20× objective fitted with dual excitation and emission filter wheels and a Photometrics CoolSNAP HQ camera. MetaMorph software (Universal Imaging; Molecular Devices, Sunnyvale, CA) was used for image acquisition and microscopic control. Images were collected in the GFP channel every 15 s for 15 min. Imaris software was used for image analysis and tracking (Bitplane, South Windsor, CT).

ATX staining

To analyze ATX receptors, cells were incubated with a preformed complex of biotin linked to ATX (b-ATX) (10 μg/ml) and PE-conjugated streptavidin (2 μg/ml) in HBSS buffer (with or without 0.5 mM Mn^{+2}) at room temperature. T cells were gated by CD3 staining. PS/2 mAb (10 μg/ml) was used to block α4 integrin.

To analyze b-ATX distribution by immunofluorescence, TK1 cells on an ICAM-1 substratum were exposed to 0.1 μM LPA. Following fixation with 4% formaldehyde, washing, and blocking, the cells were sequentially reacted with a complex of b-ATX/Cy2-streptavidin and anti-CD44 with a Cy3-conjugated secondary Ab.

Transmigration under shear flow

BEnd.3 ECs were grown to confluence in a 0.2% gelatin-coated BioFlux 48-well flow chamber plate (Fluxion Biosciences, South San Francisco, CA). Monolayers were stimulated for 16 h with TNF-α (500 U/ml). CCL21 (1 μg/ml with 0.2% fatty acid-free BSA) was overlaid on the monolayer for 5 min, followed by washing. T cells in HBSS with 0.2% fatty acid-free BSA were perfused for 2 min over the monolayer at 0.5 dyne/cm^2, and the flow was stopped for 5 min. The flow rate was then increased to 1 dyne/cm^2 for an additional 30 min. Images were recorded at one frame/10 s by video recorder. The total number of arrested cells was determined after 10 min of flow. During the 30 min of flow, lymphocytes fell into three categories: cells that moved less than two diameters (static), cells that crawled more than two cell diameters without detaching/transmigrating (crawling), and cells that became dark under phase contrast (undergoing TEM). HA130 (0.3 μM final) or BrP-LPA (10 μM final) was added in some experiments. For competition with T210A, the chamber contained a 10-fold excess of T210A relative to the indicated amount of ATX.

Statistical analysis

The unpaired Student *t* test was used to determine the statistical significance of pair-wise comparisons after satisfying *t* test criteria (33) of

equivalent variances and Gaussian distributions (approximately equal mean and median values). For comparisons of three or more groups, one-way ANOVA with the Tukey posttest was used.

Results

HA130 inhibits homing of T cells

HA130 was recently identified as a potent small-molecule inhibitor of ATX (34). The inhibitor acts to reduce both the turnover number of ATX and its affinity for LPC. We used a modified lymphocyte-homing assay to accommodate the short half-life of HA130 in blood (~3 min) (34). We injected CFSE-labeled T cells together with HA130 i.v. into mice and then reinjected the drug at 7 and 12 min. After 15 min, SLOs were sectioned and stained to reveal HEVs. $CFSE^+$ T cells were classified as either outside HEVs (in the lymphoid organ parenchyma) or within HEVs (luminal or in HEV walls). The ratio of outside HEVs to inside HEVs was used as an index of T cell migration across HEVs. In Peyer's patches, very few cells migrated into the parenchyma in 15 min, so the action of HA130 could not be evaluated. However, for PLNs and MLNs, many cells had migrated into the parenchyma (Fig. 1A). HA130 decreased the outside HEV/inside HEV ratio by 3–4-fold compared with vehicle treatment (Fig. 1B, $p < 0.01$ for both PLNs and MLNs). This result is consistent with HA130 retarding the migration of T cells across LN HEVs.

LPA and ATX/LPC polarize naive T cells

LPA induces chemokinesis of T cells in Transwell assays (30). We sought to investigate the cellular mechanisms by which LPA was exerting these effects. Stam et al. (35) reported that LPA induced the formation of pseudopods in a lymphoma cell line. To extend these findings, we examined the effects of LPA, as well as ATX, on T cells. Although T cells in the blood are round, T cells that have entered a tissue exhibit an amoeboid "hand mirror" morphology, which is characterized by a broad leading edge, a cell body with the nucleus, and a uropod at the tail (9, 36, 37). We first asked whether LPA at concentrations previously shown to be active in Transwell assays (30) could induce the polarization of TK1 cells, a mouse $CD8^+$ T cell line (38). We quantified this response by monitoring the accumulation of CD44 in uropods (37). TK1 cells were mixed with LPA at varying concentrations and allowed to settle on an ICAM-1 substratum. With no added LPA, 10% of the cells were polarized by 7 min (Fig. 2A, 2B). At 0.1 μM, the polarization was 48% and reached 78% at 10 μM. LPA at 1 μM induced maximal polarization within 5 min, with no detectable decrease after 30 min, indicating the absence of desensitization over this period (Fig. 2C).

We next investigated primary $CD3^+$ T cells, which were isolated by negative selection from LNs. At least 90% of these cells were naive defined by the criterion of $CD44^{lo}$ (data not shown), and we

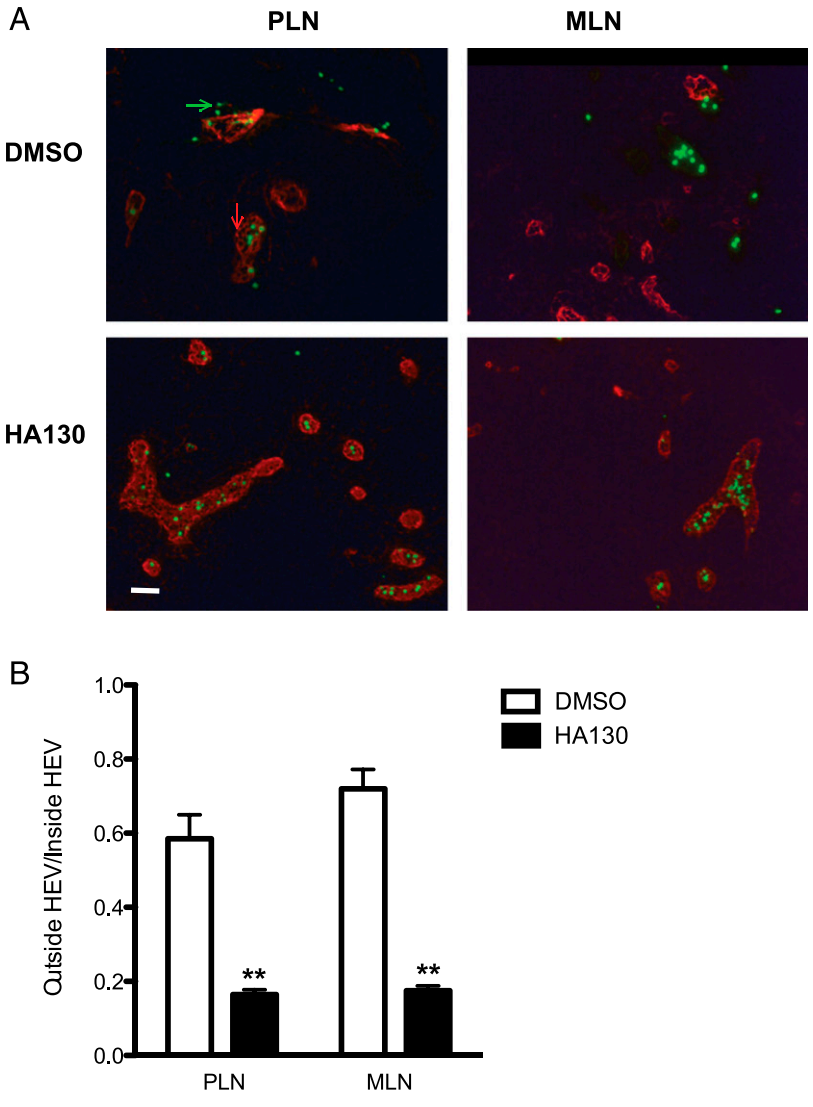

FIGURE 1. HA130 impedes T cell entry into LNs. (**A**) HEVs in PLN and MLN sections were stained with MECA-79. Representative images of CFSE-labeled T cells in control and HA130-treated mice after i.v. injection of CFSE-labeled T cells. Scale bar, 50 μM. Green arrow indicates CFSE-labeled T cell, and red arrow indicates MECA-79–stained HEV. (**B**) Bar graphs for PLN and MLN showing mean ratios ± SDs of CFSE-labeled cells outside HEV/inside HEV. Two mice were processed/experiment, with six nonconsecutive sections of two MLNs and three PLNs evaluated for each mouse. The data shown represent the pooled results from three experiments (three mice of each group). $^{**}p < 0.01$, versus DMSO control.

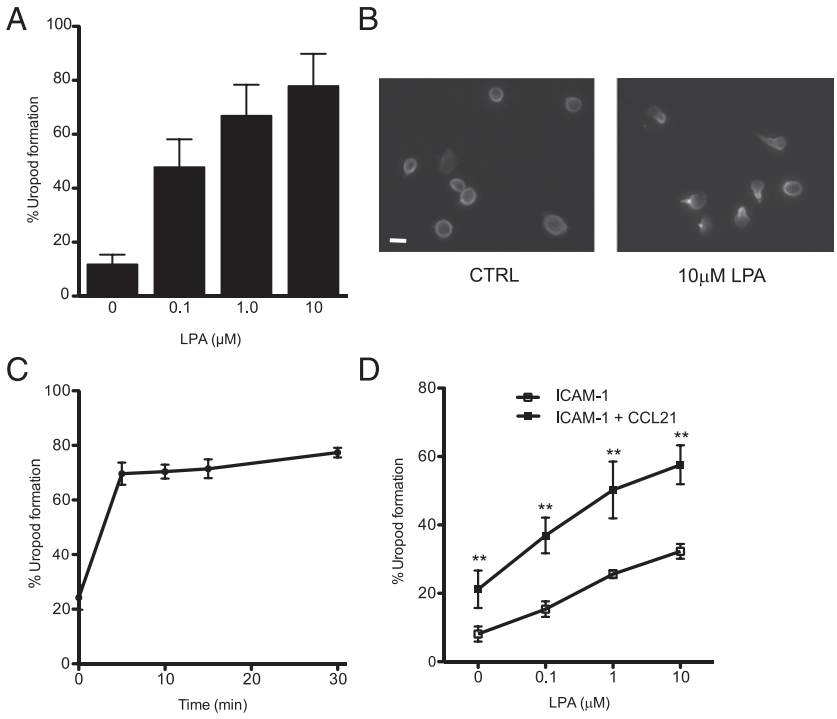

FIGURE 2. LPA induces the rapid polarization of T cells. (**A**) TK1 lymphoma cells were allowed to settle on ICAM-1 substratum in the presence of the indicated concentration of LPA. After 7 min, the percentage of cells that became polarized was determined as defined by CD44 accumulation in uropods. (**B**) CD44 staining of TK1 cells after a 7-min exposure to 10 μM LPA (*right panel*) or buffer alone (*left panel*). Scale bar, 10 μM. (**C**) Time course of TK1 polarization response to 0.1 μM LPA. (**D**) Naive mouse T cells were allowed to settle on substratum of ICAM-1 or ICAM-1 with coimmobilized CCL21 (200 ng/ml input). After 7 min, polarization was determined based on accumulation of CD43 into uropods. CD43 was used instead of CD44 because of the low expression of the latter on naive T cells. In (A), (C), and (D), means and SDs are shown and are based on three replicate wells. Data are representative of three independent experiments. $^{**}p < 0.01$, uropod formation with CCL21 versus without CCL21.

refer to this population as naive. LPA also induced polarization of these cells (Fig. 2D), with uropods identified by CD43 staining (37). LPA at 10 μM induced polarization to a maximum of 32%. Alon and coworkers (39) reported that immobilized CCL21 causes rapid polarization and motility of T cells on an adhesive substratum. Therefore, we asked what effect LPA would have on T cells that were simultaneously exposed to CCL21, which was coimmobilized with ICAM-1. CCL21 alone (200 ng/ml) induced polarization of naive T cells to 21% (Fig. 2D). Adding 10 μM LPA increased the level of polarization to 58%. A 2-fold higher level of CCL21 did not produce further augmentation (data not shown). Thus, soluble LPA and immobilized CCL21 act additively to promote uropod formation in naive T cells.

Because ATX catalyzes the production of LPA, we wanted to determine whether ATX could also induce the polarization of T cells. When we added ATX (5 μg/ml) to TK1 cells on an ICAM-1 substratum, we observed uropod formation in the presence of LPC but not in its absence (Fig. 3A). LPC at 10 μM was more effective than at 1 μM. The IC_{50} for ATX in this assay was ~0.2 μg/ml. Notably, the response to ATX/LPC was very rapid. After 30 s of exposure to 1 μg/ml of ATX, the polarization of TK1 cells doubled to 34% relative to the baseline level (Fig. 3B). By 10 min, the level of polarization reached ~75%, which was largely sustained for another 20 min.

To verify the importance of the enzymatic activity of ATX, we tested an enzymatically inactive form (T210A). There was no uropod-inducing activity by T210A at 5 μg/ml in the presence of LPC (1 μM) (Fig. 3A). We also tested two small-molecule inhibitors of ATX: HA130 (see above) and BrP-LPA (40). The latter compound is a bromophosphonate analog of LPA, which is a low micromolar inhibitor (IC_{50} ~ 0.1 μM) of ATX and antagonizes several of the LPA receptors (LPARs) (40). HA130 at 0.3 μM and BrP-LPA at 10 μM completely ablated the activity of ATX on TK1 uropod formation (Fig. 3C). However, neither had any effect on LPA-induced uropods. Thus, we conclude that BrP-LPA was able to block ATX-induced uropods by inhibiting ATX rather than LPA antagonism, which is consistent with the fact that BrP-LPA does not block all LPARs (40). Pretreatment of TK1 cells with 200 ng/ml PTX did not diminish ATX-induced polarization, indicating that the Gαi subfamily of G proteins was not involved in this response (Fig. 3D). Y27632 is a pharmacologic inhibitor of ROCK, a kinase that regulates myosin contractility (11). ROCK is an effector of RhoA, which is downstream of Gα12/13 G proteins (41). Incubation of TK1 cells with Y27632 (10 μM) completely blocked the induction of uropods by ATX (Fig. 3D).

We next examined primary naive $CD3^+$ T cells and found that ATX in combination with LPC also induced their polarization (Fig. 3E). As with LPA, the action of ATX on uropod formation was additive to that of immobilized CCL21. Without LPC, ATX did not augment polarization. ATX, as well as LPA, also induced the polarization of primary human T cells and neutrophils from peripheral blood (Fig. 3F). Neutrophil polarization by LPA was reported previously (42).

ATX receptors on T cells

Our previous work showed that human T cells can bind to plastic-immobilized ATX in an α4β1-dependent manner (30). We found that CCL21 stimulation of T cells or the addition of Mn^{+2} (which globally activate integrins) greatly augments α4β1-dependent binding, suggesting that ATX binding requires the active conformation of α4β1 (30). Similarly, activated β1 and β3 integrins on platelets are required to bind ATX (43). Although Mn^{+2} increases the binding of mouse T cells to immobilized ATX, we were unable to implicate the involvement of any particular integrin (30). To further study ATX receptors on lymphocytes, we linked biotin to ATX (b-ATX) to generate a soluble probe. Consistent with previous observations (30), naive $CD3^+$ T cells showed increased b-ATX staining in the presence of Mn^{+2} (Fig. 4A), as did $CD4^+$ and $CD8^+$ subsets of T cells as well as B cells (Supplemental Fig. 1). A neutralizing Ab to α4β1 (PS/2) did not diminish staining of T cells (Fig. 4B), and T cells from β2- and β3-null mice did not show reduced staining compared with wild-type T cells (Fig. 4C). b-ATX staining of T cells was inhibited >90% by the addition of a 10-fold excess of T210A, verifying that the receptors were saturable (Fig. 4D). Staining of rounded TK1 cells with b-ATX

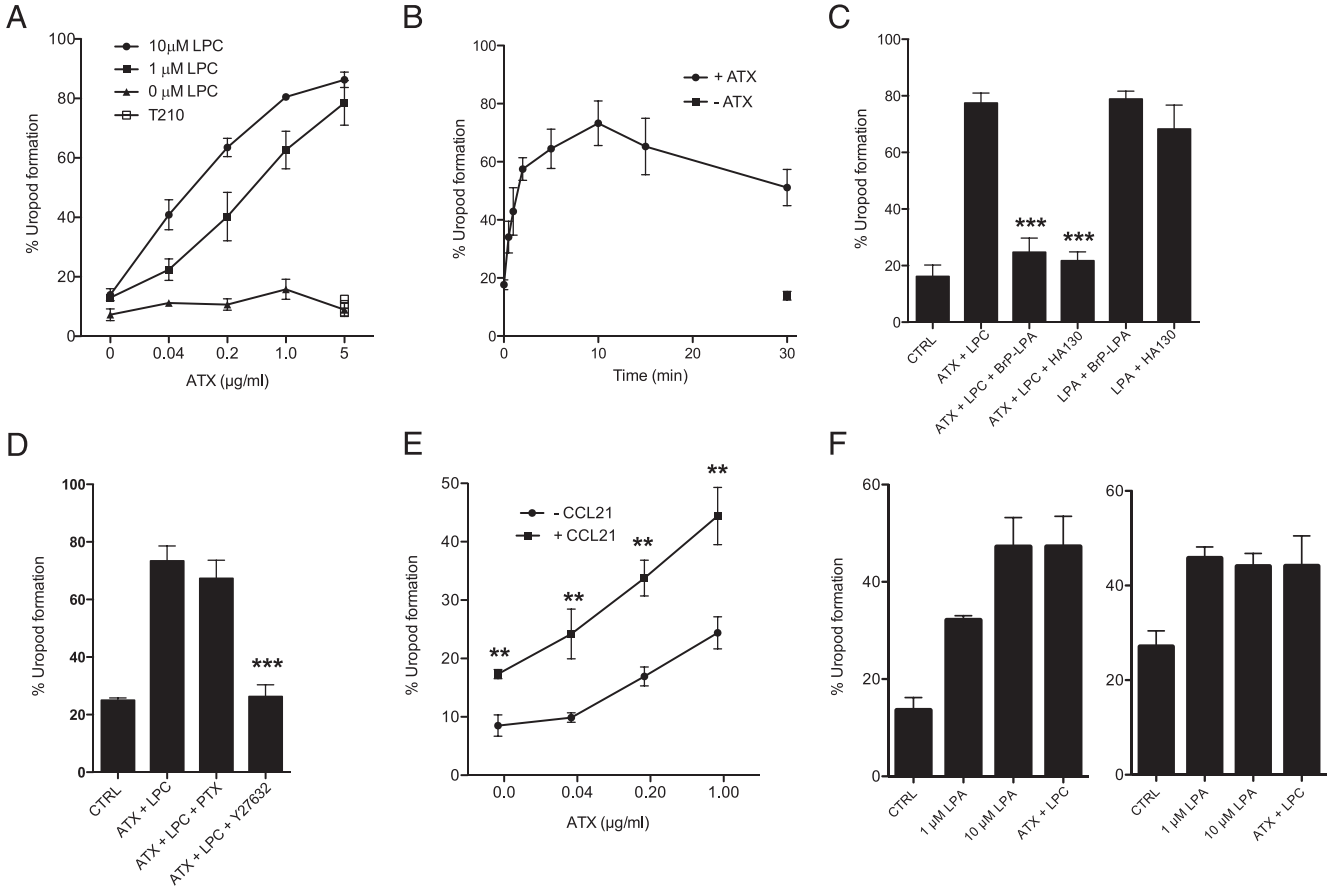

FIGURE 3. ATX in the presence of LPC induces polarization of T cells. (**A**) TK1 cells were allowed to settle on ICAM-1 substratum in the presence of the indicated concentration of ATX, with (1 or 10 μM) or without LPC in solution . □, response to 5 μg/ml of T210A with 10 μM LPC. After 7 min, the percentage of cells that became polarized was determined by CD44 accumulation in uropods. For all ATX concentrations, with the exception of 5 μg/ml: 10 μM LPC > 1 μM > 0 LPC; $p < 0.01$, ANOVA. For 5 μg/ml ATX: 1 and 10 μM LPC > 0 LPC; $p < 0.001$, ANOVA. (**B**) Time course of TK1 polarization response to 1 μg/ml ATX and 1 μM LPC in solution. ■, response to 1 μM LPC alone. (**C**) TK1 polarization response to ATX (5 μg/ml) plus LPC (1 μM) or to LPA (1 μM) in the presence of either BrP-LPA (10 μM) or HA130 (0.3 μM). Uropod response was measured after 7 min. ***$p < 0.001$, ATX/LPC versus ATX/LPC + HA130 or versus ATX/LPC + BrP-LPA. (**D**) TK1 polarization response to ATX (5 μg/ml) plus LPC (1 μM) when cells were treated with PTX (200 ng/ml) or Y27632 (10 μM). ***$p < 0.001$, ATX/LPC versus ATX/LPC + Y27632. (**E**) Naive T cell polarization response (CD43 uropod assay) to the indicated concentration of ATX in solution with 1 μM LPC present. The substratum consisted of ICAM-1 with or without coimmobilized CCL21 (200 ng/ml). **$p < 0.01$, uropod formation with CCL21 versus without CCL21. (**F**) Human blood T cells (*left panel*) and neutrophils (*right panel*) were allowed to settle on ICAM-1–coated wells in the presence of LPA or ATX (1 μg/ml) with 1 μM LPC. Uropod formation was determined by staining for the accumulation of CD44. In all panels, means and SDs are shown and are based on three replicate wells. Data are representative of three independent experiments, with the exception of (F), for which experiments were performed twice. CTRL, No additions.

revealed a patchy distribution around the cells. Upon LPA-induced polarization of TK1 cells, b-ATX staining was greatly enriched at the leading edge of cells opposite from the CD44-stained uropod (Fig. 4E).

LPA and ATX/LPC induce motility of naive T cells

Because a polarized morphology is a requirement for active leukocyte migration (9, 36, 37), we performed motility assays. In this study, we used $CD4^+$ T cells, of which ≥95% were naive. Using a custom chamber for visualizing two-dimensional cell behavior, we found that 1 μM LPA augmented $CD4^+$ T cell migration on a substratum of coimmobilized ICAM-1 and CCL21 (Fig. 5). LPA induced a 26% increase in median velocity, from 4.72 to 5.96 μm/min ($p < 0.0001$, Fig. 5A). Furthermore, the LPA-treated cells exhibited a marked shift to smaller median turning angles (81.3 versus 51.1°, $p < 0.0001$) (Fig. 5B), indicating a greater tendency to move in a straight line. These effects persisted for ≥60 min following exposure to LPA (data not shown).

We next investigated ATX in the migration chamber (Fig. 6). Consistent with the previous report (39), immobilized CCL21 promoted naive T cell migration on ICAM-1, as measured by increased velocity (2.43 versus 5.49 μm/min, $p < 0.001$) (Fig. 6E), decreased turning angles (90.2 versus 76.8°, $p < 0.001$) (Fig. 6F), and increased net displacement (2.73 versus 13.9 μm/10 min, $p < 0.001$) (Fig. 6G). Similarly, ATX/LPC produced comparable effects on the velocity (2.43 versus 4.59 μm/min, $p < 0.001$) (Fig. 6E), turning angle (90.2 versus 68.5°, $p < 0.001$) (Fig. 6F), and net displacement (2.73 versus 15.2 μm/10 min, $p < 0.001$) (Fig. 6G) of T cells compared with the no-stimulant condition. Finally, the effects of both treatments together on migration were additive. The median velocity of 8.05 μm/min (with 25% above 11.05 μm/min) in the presence of both stimulants (Fig. 6E) is comparable to median velocities of 5.7–15.1 μm/min observed for interstitial T cell migration within LNs (44–46). Our findings establish that naive T cell polarization induced by LPA or ATX/LPC is indeed translated into motility.

LPA and ATX/LPC promote TEM of T cells under shear stress

Arrested lymphocytes on HEVs experience the shear stress of blood flow as they crawl on the luminal aspects of the endothelium prior

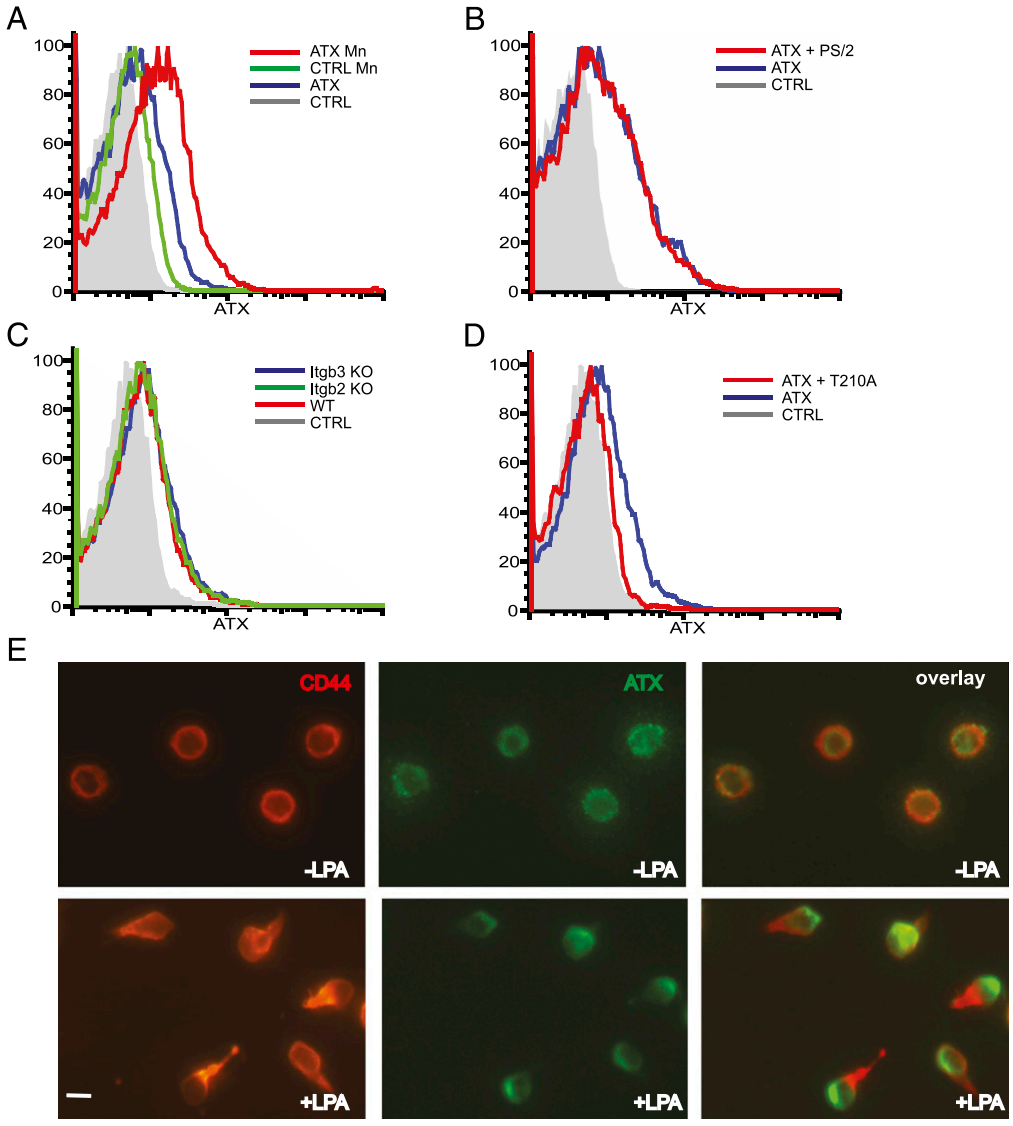

FIGURE 4. Binding of ATX to T cells. (**A**) Flow cytometry analysis of b-ATX staining of mouse T cells in the presence (red) or absence (blue) of Mn^{+2}. (**B**) b-ATX staining (with Mn^{+2} present) of T cells in the presence or absence of PS/2, an anti-α4 integrin Ab. (**C**) b-ATX staining (with Mn^{+2} present) of T cells from wild-type mice, β2-deficient T cells (*ltgβ2* null mice), and β3-deficient T cells (*ltgβ3* null mice). (**D**) b-ATX staining (with Mn^{+2} present) of T cells in the presence or absence of a 10-fold excess of T210A. (**E**) Fluorescent imaging of TK1 cells stained with b-ATX (green) and CD44 (red). Rounded cells bound to substratum (*upper panels*) and polarized cells (induced with 1 μM LPA) (*lower panels*). Scale bar, 10 μM. Data are representative of at least four independent experiments. CTRL, Staining with b-ATX omitted.

to TEM. We turned to a previously described ex vivo system to investigate lymphocyte migration on an EC monolayer and TEM under physiologic shear flow (13, 47). In this model, bEnd.3 ECs are cultured on the bottom of a flow chamber and treated with TNF-α to induce expression of integrin counter-receptors. The EC monolayer is apically exposed to an arrest chemokine, such as CCL21 or CXCL12, and lymphocytes are allowed to interact with the monolayer at low shear stress. This step circumvents the physiologic rolling step, in which slowly moving lymphocytes encounter arrest chemokines. Upon application of shear stress to the system, the lymphocytes stick via activated integrins (13). They then undergo TEM, with the vast majority of the cells crossing the endothelial barrier by the paracellular route (47). We allowed $CD3^+$ T cells to settle on TNF-α–activated and CCL21-coated bEnd.3 ECs and then applied shear (1 dyne/cm^2). After 10 min, we observed robust shear-resistant adhesion of T cells (Fig. 7A). Without CCL21 treatment, 5-fold fewer T cells bound to the monolayer. Consistent with previous findings (13), inclusion of an anti-β2 mAb reduced the number of adherent cells (shear resistant) by ~75%, and the further addition of an anti–MAdCAM-1 mAb reduced adhesion by 95%. After an additional 20 min of flow, ~5% of the adherent T cells had completed TEM, as judged by the appearance of phase-dark cells under the monolayer. When we added LPA to the chamber, there was a dose-dependent increase in the number of transmigrated cells, from 5% with no added LPA to 20% with 10 μM LPA (Fig. 7B). With ATX added instead of LPA, there was a dose-dependent increase in TEM in the presence of LPC; 1 μg/ml ATX with 1 μM LPC produced a 6-fold increase to 30% (Fig. 7C). Without LPC, ATX did not change the level of TEM from baseline, and LPC without ATX also had no effect. Categorizing the behavior of cells, we found that 1 μg/ml ATX (1 μM LPC) reduced the percentage of static T cells by >50% and increased the percentage of cells undergoing TEM by 6-fold, without altering the percentage of cells that crawled intraluminally (Fig. 7D). To substantiate that ATX enzymatic activity was essential, we tested the T210A mutant and found that

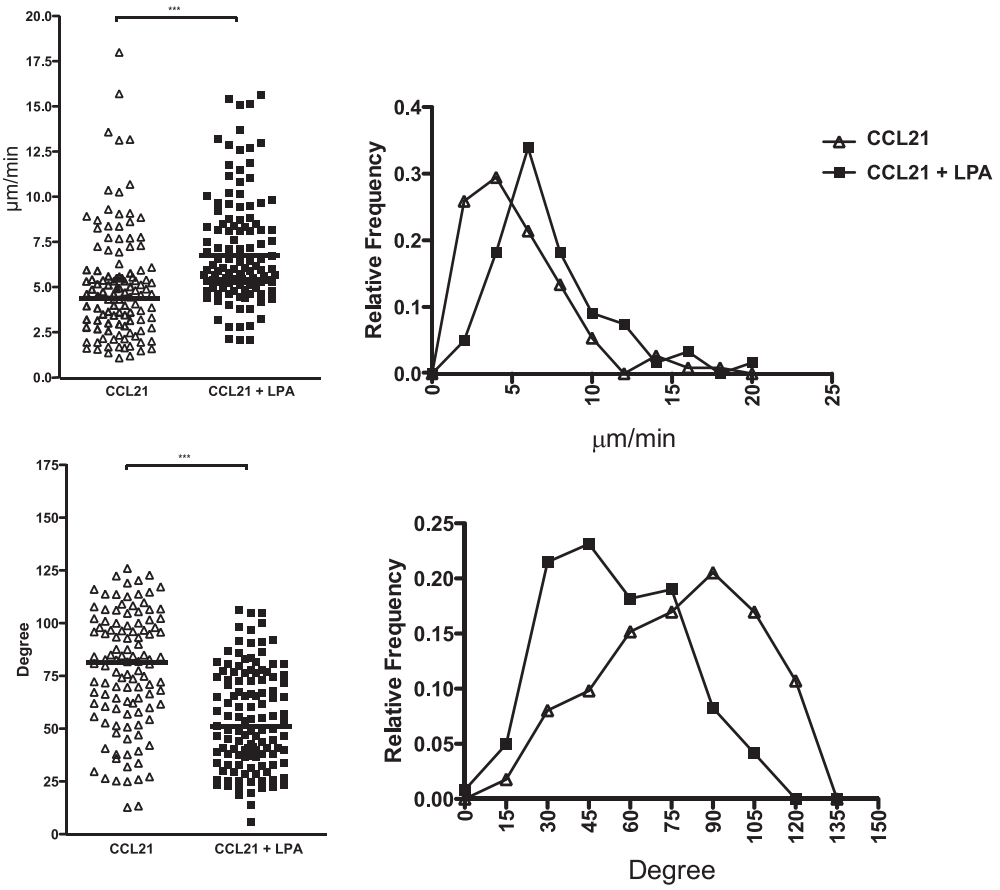

FIGURE 5. LPA induces motility of naive T cells. Naive GFP$^+$ CD4$^+$ OTII T cells were seeded, with or without 1 μM LPA, onto a chamber coated with ICAM-1 and CCL21. Median velocity (*upper panels*) and turning angle (*lower panels*) of each cell were measured and are shown in dot plots and relative frequency plots. Data are representative of three independent experiments. ***$p < 0.001$.

it was inactive at 5 μg/ml (Fig. 7E). Furthermore, both HA130 and BrP-LPA abolished the enhancing effect of ATX on TEM (Fig. 7E). However, BrP-LPA had no effect on LPA-induced TEM (data not shown). To confirm that naive cells within the CD3$^+$ T cell population were responding in this assay, we further purified the cells by negative selection for CD44. ATX/LPC induced the same extent of TEM by this enriched population (≥99% naive) as that observed for parental cells (90% naive) (Supplemental Fig. 2).

The bEnd.3 system provided the opportunity to model the previous in vivo observation that i.v. injection of T210A markedly reduced T cell homing (30). Our interpretation was that the inactive ATX displaced endogenous ATX from T cells and prevented the local production of motility-enhancing LPA in the vicinity of the cells. Because T210A competes the binding of ATX to T cells (Fig. 4D), inclusion of an excess of T210A relative to ATX in the flow chamber allowed us to determine whether the active enzyme had to bind to T cells to stimulate TEM. We tested two concentrations of ATX with or without a 10-fold excess of T210A (Fig. 7F). At 5 μg/ml of ATX, 28% of the arrested T cells completed TEM during the 30-min period of flow. The inclusion of 50 μg/ml of T210A reduced TEM to 16%. ATX at 0.5 μg/ml stimulated 12% TEM. Inclusion of 5 μg/ml of T210A reduced TEM to the background level. These results indicate that binding of ATX to T cells is required for optimal TEM-promoting activity.

Discussion

Our previous study demonstrated the activity of LPA on primary mouse and human T cells in a Transwell assay (30). Because lymphocytes normally migrate in contact with other cells (e.g., endothelium) or extracellular matrix, the Transwell assay was not informative about whether LPA could induce motility responses in T cells on a biologically relevant substratum. In the present investigation, we found that LPA promoted the transformation of T cells on an ICAM-1 substratum from a rounded shape to a polarized morphology with a well-defined leading edge and uropod (Fig. 2). The distinctive hand mirror morphology is a prerequisite for active cell migration of leukocytes (36, 37). Consistent with this, we verified that LPA induced motility of naive T cells on an ICAM-1 substratum (Fig. 5). Surface-bound CCL21 also promoted motility of these cells, as previously reported (39), and soluble LPA and immobilized CCL21 functioned additively.

It was critical to determine whether ATX could serve as a source of LPA in these assays. Indeed, ATX/LPC added to TK1 cells efficiently induced their polarization (Fig. 3). PTX treatment had no effect on this response, in contrast to its abrogation of CCL21-induced polarization and motility of lymphocytes (39). ATX/LPC was also active on naive T cells, inducing both their polarization and motility, and these cells also responded additively to CCL21 and ATX/LPC (Figs. 3, 6). Several studies reported that the random migration of T cells within LNs strongly depends on Gαi signaling (44, 45). Contributing to this motility are CCR7 and its ligands (CCL21 and CCL19) (44–46). Interestingly, a component of T cell motility remains after complete PTX inhibition of Gαi signaling, implicating a chemokine-independent mechanism (44, 45). Notably, ATX transcripts and protein are detected within the parenchyma of LNs, in addition to their very high expression in HEVs (30). A topic for further study is whether LPA produced by extravascular

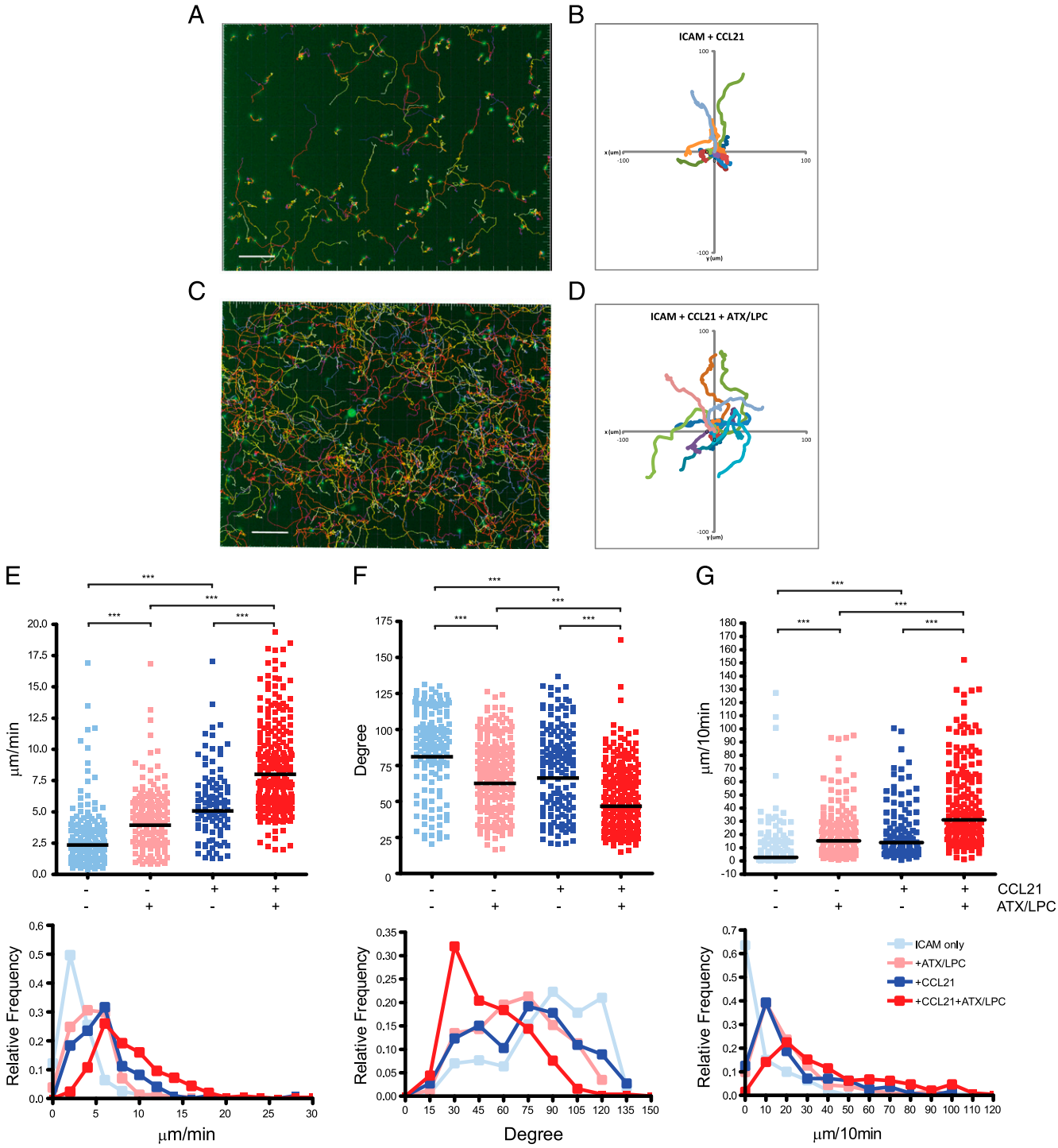

FIGURE 6. ATX induces motility of naive T cells. Naive GFP$^+$ CD4$^+$ OTII T cells were seeded onto a crawling chamber coated with 3 μg/ml ICAM-1 + 400 ng/ml CCL21, with or without 1 μg/ml ATX plus 10 μM LPC in solution. T cells were imaged every 15 s for 15 min and tracked by Imaris software. Cell tracks are shown for a 10-min period on an ICAM-1 plus CCL21 substratum (**A**, **B**) and on an ICAM-1 plus CCL21 substratum in the presence of 1 μg/ml ATX and 10 μM LPC in solution (**C**, **D**). (A) and (C) show all of the tracks (>100 cells/experimental set) (scale bars, 100 μM); (B) and (D) show 10 randomly chosen sample tracks for a 10-min period of migration referenced to the origin of each cell. Median velocity (**E**), turning angle (**F**), and average total displacement (**G**) of each cell were measured over 10 min and are shown in dot plots (*upper panels*) and relative frequency plots (*lower panels*). Data are representative of three independent experiments. ***$p < 0.001$, ANOVA.

ATX influences the migration and positioning of lymphocytes within lymphoid organs.

Although the above findings have implications for extravascular migration of lymphocytes under no-shear conditions, our primary interest was the contribution of ATX/LPA to T cell interactions with HEVs under blood flow conditions. To model these events, we used cytokine-activated bEnd.3 ECs in a flow chamber with apically displayed CCL21 (Fig. 7). Previous work with this model documented integrin-dependent sticking of lymphocytes, followed by a migratory phase in the which lymphocytes polarize, migrate on the EC surface, and finally undergo TEM (13, 47). The timing and molecular requirements for these steps in this ex vivo system closely parallel those established for T cell homing across HEVs in vivo (11, 48, 49).

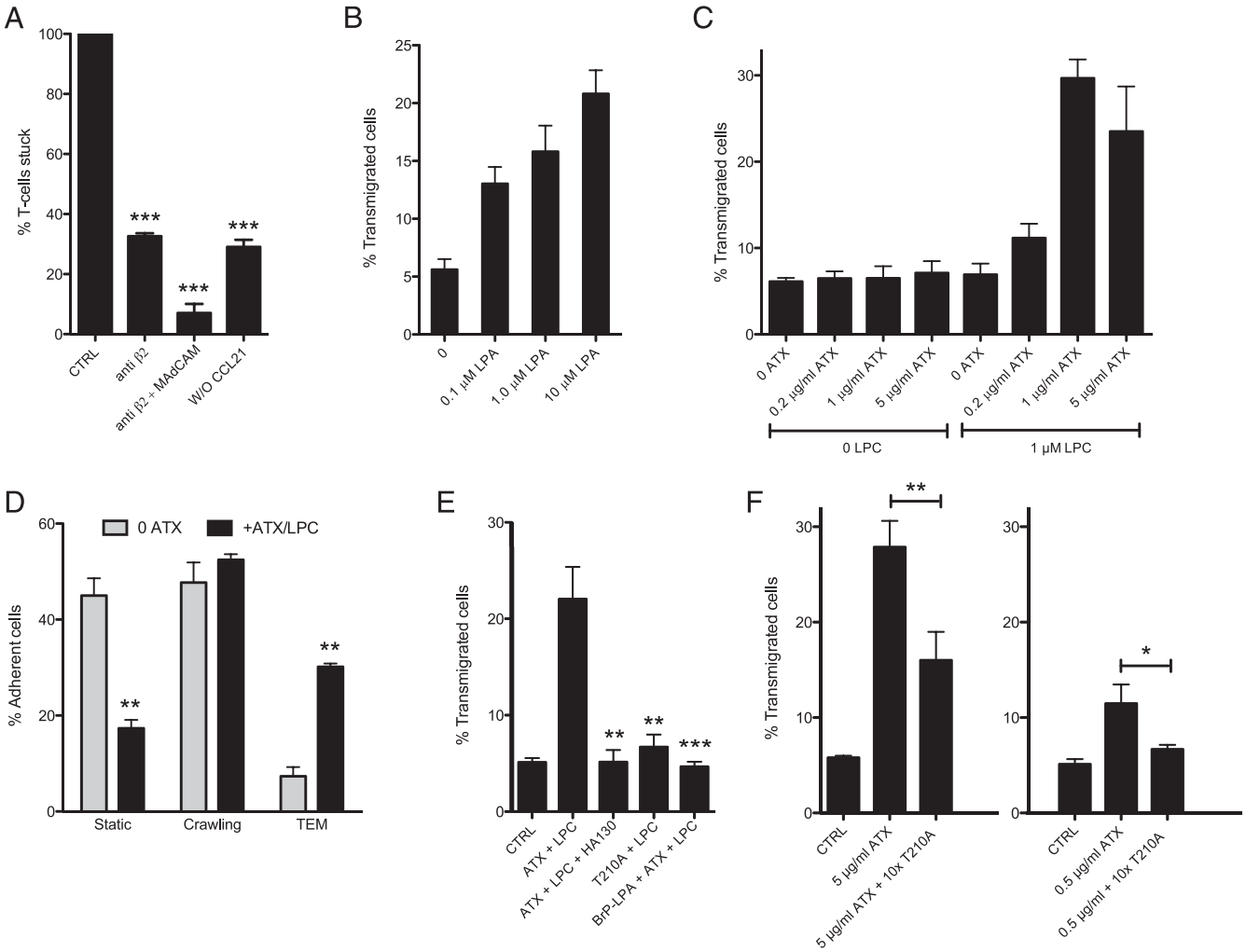

FIGURE 7. LPA and ATX promote TEM of T cells in a flow chamber. (**A**) Mouse T cells were allowed to adhere to TNF-α–stimulated and CCL21-coated bEnd.3 cells under shear stress in the presence of buffer alone (CTRL), anti-β2 integrin Ab, and anti-MAdCAM-1 Ab or without CCL21 pretreatment of the EC monolayer. After a 10-min period of flow, the number of adherent T cells was normalized to the number of adherent cells with buffer alone. ***$p < 0.001$, compared with CTRL. (**B**) LPA was added to the flow chamber, and the number of T cells undergoing TEM across the bEnd.3 monolayer was determined over the 30-min period of flow and computed as a percentage of the number of adherent cells at 10 min. (**C**) ATX was added to the chamber, with or without LPC, and the number of T cells undergoing TEM was determined as above. (**D**) The flow chamber contained either buffer or ATX (5 μg/ml) plus LPC (1 μM). The behavior of adherent T cells was categorized as static, crawling, or undergoing TEM. The percentage of cells in each category, with or without ATX/LPC, was compared. **$p < 0.01$, ATX/PLC versus no treatment. (**E**) TEM of T cells across the bEnd.3 monolayer was measured in the presence of buffer alone (CTRL), ATX/LPC (5 μg/ml/1 μM), ATX/LPC plus HA130 (0.3 μM), ATX/LPC plus BrP-LPA (10 μM), or T210A/LPC (5 μg/ml/1 μM). **$p < 0.01$, ***$p < 0.001$, versus treatment with ATX/LPC. (**F**) TEM of T cells across the bEnd.3 monolayer was measured as above in the presence of buffer alone (CTRL), 5 μg/ml ATX, 5 μg/ml ATX plus 10-fold T210A, 0.5 μg/ml ATX, or 0.5 μg/ml ATX plus 10-fold excess of T210A. The data shown in the two panels are from separate experiments. All ATX conditions also included 1 μM LPC. Means and SDs are shown and are based on three replicate determinations. Data are representative of three independent experiments. *$p < 0.05$, **$p < 0.01$.

Using this system, we found that LPA or ATX/LPC induced a 4–6-fold increase in naive T cells that underwent TEM. Interestingly, the number of crawling cells was not increased by exposure to ATX/LPC. Thus, under flow, ATX does not appear to affect the conversion of arrested cells to migrating cells but rather increases the efficiency of TEM. Of note, Park et al. (49) found that mutant T cells that are unable to downregulate LFA-1 affinity exhibit reduced diapedesis across HEVs. Furthermore, pharmacologic impairment of uropod contractility slows TEM of T cells across both HEVs in vivo and cultured endothelium, probably because release of the adherent uropod is impaired (11, 50). These studies highlight the importance of integrin de-adhesion during lymphocyte TEM and raise the possibility that LPA signaling may be involved in downregulation of LFA-1 affinity.

ATX is a large multidomain protein, and it is conceivable that it could modulate T cell migration through a nonenzymatic mechanism. In fact, Zhao et al. (51) found that T210A could stimulate the motility of airway epithelial cells. We established that ATX was exerting its effects on T cell TEM via its enzymatic activity by showing that there was no TEM-promoting activity by LPC alone, by ATX in the absence of LPC, or by T210A. Furthermore, both HA130 and BrP-LPA completely blocked the ability of ATX to promote TEM. This ex vivo finding with HA130 complements the observation that this ATX antagonist also impeded the migration of T cells of lymphocytes across HEVs in vivo (Fig. 1).

ATX was originally thought to be a type II transmembrane protein and was proposed to be released from the cell surface by shedding (16). Subsequently, ATX was shown to be a true secre-

tory protein, which is processed at its N terminus by the removal of a signal sequence and furin-mediated cleavage (17). We used b-ATX to verify the presence of ATX receptors on mouse T cells (Fig. 4). Although ATX binding was enhanced by Mn^{+2}, we could not directly implicate the involvement of particular integrins, as was reported for human T cells ($\alpha4\beta1$) (30) and platelets ($\beta1$ and $\beta3$) (43).

Nonetheless, we were still able to support the functional relevance of ATX binding to T cells in the bEnd.3 system. Thus, we found that ATX-stimulated TEM was markedly reduced when ATX was added in the presence of a 10-fold excess of T210A, a condition that reduced the level of ATX associated with the surface of T cells but did not change the amount of active enzyme in the flow chamber (Fig. 7). This ex vivo result rationalizes and complements the previous in vivo demonstration that i.v. administration of T210A inhibits lymphocyte homing (30).

Two mutually nonexclusive mechanisms can be envisioned for how ATX binding to T cells potentiates its TEM-promoting activity. First, the crystal structure of ATX reveals a hydrophobic channel, which is thought to serve as conduit for the passage of LPA from the active site of the enzyme to an exit site on the surface of the enzyme (52, 53). Because the exit site is predicted to be at the interface of ATX with its cellular binding partner, the hydrophobic channel could be the basis for a shuttling mechanism to transfer LPA close to its signal-transduction receptors on the partner cell (52, 53). Notably, we detected ATX binding at the leading edge of lymphocytes where many chemoreceptors are localized (37). An additional refinement to enhance signaling would be an actual physical association between ATX and LPAR. In fact, lung epithelial cells, which migrate in response to ATX, exhibit a cell surface complex of ATX with LPA1 and $\beta4$ integrin (51). The existence of an analogous complex on lymphocytes would be predicted to facilitate shuttling of LPA to its LPARs so as to counteract the dissipative action of blood flow on focally generated LPA and to sequester LPA from the action of lipid phosphate phosphatases in the blood. A second possible mechanism for potentiation is that the interaction of ATX with its receptors on T cells activates the enzyme, as appears to occur when ATX binds to activated platelets (43).

Although the current study establishes an important role for the ATX–LPA signaling axis in T cell migration, the relevant LPARs remain to be identified. Of the six LPARs, four (LPA2, LPA4, LPA5, and LPA6) are expressed at the transcript level in populations of mouse T cells, as determined by mining of the Immunological Genome Project database (http://www.immgen.org). Functions other than cell migration are served by lymphocyte LPARs (e.g., in cytokine secretion, cell proliferation, and cell survival) (54). TK1 cells express transcripts for LPA2, LPA5, and LPA6 (data not shown). Because Y27632 prevented the polarization response of this cell type to ATX/LPC (Fig. 3D), the $G\alpha12/13$–Rho axis is implicated in the signaling pathway (41). All three of the LPARs present in TK1 cells can couple to this class of G proteins (19, 55). Importantly, our findings that 10 μM BrP-LPA did not inhibit either LPA-induced polarization or LPA-induced TEM argues against the involvement of LPA1–4 in these responses, because BrP-LPA antagonizes these receptors with submicromolar Ki's (56). Interestingly, BrP-LPA is a weak agonist of LPA5 (40). Thus, LPA5 and LPA6 (not yet investigated with BrP-LPA) are of interest with respect to their potential roles in the polarization and TEM of T cells. Clearly, the endothelium is not a passive partner during TEM, and locally produced LPA may also signal through LPARs on ECs during the process (31).

Sphingosine 1-phosphate (S1P) and LPA are closely related lysophospholipids, both having a three-carbon scaffold, a phosphate head group, and a single fatty acid chain (20). Like LPA, S1P signals through multiple GPCRs (20). Notably, S1P regulates the efflux of lymphocytes from LNs into lymph (57, 58). The present study substantiates a role for LPA in the entry of blood-borne lymphocytes into LNs and, thus, expands the functions of extracellular lysophospholipids in leukocyte trafficking.

Acknowledgments

We thank Drs. Harald Albers, Huib Ovaa, and Wouter Moolenaar of the Netherlands Cancer Institute for generously providing HA130 prior to its commercial availability. Preliminary experiments on LPA-induced polarization of lymphocytes were conducted by Hidenobu Kanda and Yuka Morita.

Disclosures

The authors have no financial conflicts of interest.

References

1. Gowans, J. L., and E. J. Knight. 1964. The route of recirculation of lymphocytes in the rat. *Proc. R. Soc. Lond. B Biol. Sci.* 159: 257–282.
2. Butcher, E. C., and L. J. Picker. 1996. Lymphocyte homing and homeostasis. *Science* 272: 60–66.
3. Ruddle, N. H., and E. M. Akirav. 2009. Secondary lymphoid organs: responding to genetic and environmental cues in ontogeny and the immune response. *J. Immunol.* 183: 2205–2212.
4. Girard, J.-P., and T. A. Springer. 1995. High endothelial venules (HEVs): specialized endothelium for lymphocyte migration. *Immunol. Today* 16: 449–457.
5. von Andrian, U. H., and T. R. Mempel. 2003. Homing and cellular traffic in lymph nodes. *Nat. Rev. Immunol.* 3: 867–878.
6. Ley, K., C. Laudanna, M. I. Cybulsky, and S. Nourshargh. 2007. Getting to the site of inflammation: the leukocyte adhesion cascade updated. *Nat. Rev. Immunol.* 7: 678–689.
7. Rosen, S. D. 2004. Ligands for L-selectin: homing, inflammation, and beyond. *Annu. Rev. Immunol.* 22: 129–156.
8. Alon, R., and Z. Shulman. 2011. Chemokine triggered integrin activation and actin remodeling events guiding lymphocyte migration across vascular barriers. *Exp. Cell Res.* 317: 632–641.
9. Thelen, M., and J. V. Stein. 2008. How chemokines invite leukocytes to dance. *Nat. Immunol.* 9: 953–959.
10. Hogg, N., I. Patzak, and F. Willenbrock. 2011. The insider's guide to leukocyte integrin signalling and function. *Nat. Rev. Immunol.* 11: 416–426.
11. Soriano, S. F., M. Hons, K. Schumann, V. Kumar, T. J. Dennier, R. Lyck, M. Sixt, and J. V. Stein. 2011. In vivo analysis of uropod function during physiological T cell trafficking. *J. Immunol.* 187: 2356–2364.
12. Cinamon, G., V. Shinder, and R. Alon. 2001. Shear forces promote lymphocyte migration across vascular endothelium bearing apical chemokines. *Nat. Immunol.* 2: 515–522.
13. Shulman, Z., R. Pasvolsky, E. Woolf, V. Grabovsky, S. W. Feigelson, N. Erez, Y. Fukui, and R. Alon. 2006. DOCK2 regulates chemokine-triggered lateral lymphocyte motility but not transendothelial migration. *Blood* 108: 2150–2158.
14. Palmeri, D., F. R. Zuo, S. D. Rosen, and S. Hemmerich. 2004. Differential gene expression profile of human tonsil high endothelial cells: implications for lymphocyte trafficking. *J. Leukoc. Biol.* 75: 910–927.
15. Stracke, M. L., H. C. Krutzsch, E. J. Unsworth, A. Arestad, V. Cioce, E. Schiffmann, and L. A. Liotta. 1992. Identification, purification, and partial sequence analysis of autotaxin, a novel motility-stimulating protein. *J. Biol. Chem.* 267: 2524–2529.
16. Murata, J., H. Y. Lee, T. Clair, H. C. Krutzsch, A. A. Arestad, M. E. Sobel, L. A. Liotta, and M. L. Stracke. 1994. cDNA cloning of the human tumor motility-stimulating protein, autotaxin, reveals a homology with phosphodiesterases. *J. Biol. Chem.* 269: 30479–30484.
17. Jansen, S., C. Stefan, J. W. Creemers, E. Waelkens, A. Van Eynde, W. Stalmans, and M. Bollen. 2005. Proteolytic maturation and activation of autotaxin (NPP2), a secreted metastasis-enhancing lysophospholipase D. *J. Cell Sci.* 118: 3081–3089.
18. Umezu-Goto, M., Y. Kishi, A. Taira, K. Hama, N. Dohmae, K. Takio, T. Yamori, G. B. Mills, K. Inoue, J. Aoki, and H. Arai. 2002. Autotaxin has lysophospholipase D activity leading to tumor cell growth and motility by lysophosphatidic acid production. *J. Cell Biol.* 158: 227–233.
19. Choi, J. W., D. R. Herr, K. Noguchi, Y. C. Yung, C.-W. Lee, T. Mutoh, M.-E. Lin, S. T. Teo, K. E. Park, A. N. Mosley, and J. Chun. 2010. LPA receptors: subtypes and biological actions. *Annu. Rev. Pharmacol. Toxicol.* 50: 157–186.
20. Blaho, V. A., and T. Hla. 2011. Regulation of mammalian physiology, development, and disease by the sphingosine 1-phosphate and lysophosphatidic acid receptors. *Chem. Rev.* 111: 6299–6320.
21. Okudaira, S., H. Yukiura, and J. Aoki. 2010. Biological roles of lysophosphatidic acid signaling through its production by autotaxin. *Biochimie* 92: 698–706.
22. Tanaka, M., S. Okudaira, Y. Kishi, R. Ohkawa, S. Iseki, M. Ota, S. Noji, Y. Yatomi, J. Aoki, and H. Arai. 2006. Autotaxin stabilizes blood vessels and is required for embryonic vasculature by producing lysophosphatidic acid. *J. Biol. Chem.* 281: 25822–25830.

23. van Meeteren, L. A., P. Ruurs, C. Stortelers, P. Bouwman, M. A. van Rooijen, J. P. Pradère, T. R. Pettit, M. J. Wakelam, J. S. Saulnier-Blache, C. L. Mummery, et al. 2006. Autotaxin, a secreted lysophospholipase D, is essential for blood vessel formation during development. *Mol. Cell. Biol.* 26: 5015–5022.
24. Tomsig, J. L., A. H. Snyder, E. V. Berdyshev, A. Skobeleva, C. Mataya, V. Natarajan, D. N. Brindley, and K. R. Lynch. 2009. Lipid phosphate phosphohydrolase type 1 (LPP1) degrades extracellular lysophosphatidic acid in vivo. *Biochem. J.* 419: 611–618.
25. Kishimoto, T., T. Matsuoka, S. Imamura, and K. Mizuno. 2003. A novel colorimetric assay for the determination of lysophosphatidic acid in plasma using an enzymatic cycling method. *Clin. Chim. Acta* 333: 59–67.
26. Smyth, S. S., H. Y. Cheng, S. Miriyala, M. Panchatcharam, and A. J. Morris. 2008. Roles of lysophosphatidic acid in cardiovascular physiology and disease. *Biochim. Biophys. Acta* 1781: 563–570.
27. Houben, A. J., and W. H. Moolenaar. 2011. Autotaxin and LPA receptor signaling in cancer. *Cancer Metastasis Rev.* 30: 557–565.
28. Nikitopoulou, I., N. Oikonomou, E. Karouzakis, I. Sevastou, N. Nikolaidou-Katsaridou, Z. Zhao, V. Mersinias, M. Armaka, Y. Xu, M. Masu, et al. 2012. Autotaxin expression from synovial fibroblasts is essential for the pathogenesis of modeled arthritis. *J. Exp. Med.* 209: 925–933.
29. Emo, J., N. Meednu, T. J. Chapman, F. Rezaee, M. Balys, T. Randall, T. Rangasamy, and S. N. Georas. 2012. Lpa2 is a negative regulator of both dendritic cell activation and murine models of allergic lung inflammation. *J. Immunol.* 188: 3784–3790.
30. Kanda, H., R. Newton, R. Klein, Y. Morita, M. D. Gunn, and S. D. Rosen. 2008. Autotaxin, an ectoenzyme that produces lysophosphatidic acid, promotes the entry of lymphocytes into secondary lymphoid organs. *Nat. Immunol.* 9: 415–423.
31. Nakasaki, T., T. Tanaka, S. Okudaira, M. Hirosawa, E. Umemoto, K. Otani, S. Jin, Z. Bai, H. Hayasaka, Y. Fukui, et al. 2008. Involvement of the lysophosphatidic acid-generating enzyme autotaxin in lymphocyte-endothelial cell interactions. *Am. J. Pathol.* 173: 1566–1576.
32. Wijesinghe, D. S., E. K. Mayton, J. A. Mietla, A. Mukherjee, J. Wu, X. Fang, and C. E. Chalfant. 2011. Characterization of lysophosphatidic acid subspecies produced by autotaxin using a modified HPLC ESI-MS/MS method. *Anal. Methods* 3: 2822–2828.
33. Lamb, T. J., A. L. Graham, and A. Petrie. 2008. T testing the immune system. *Immunity* 28: 288–292.
34. Albers, H. M., A. Dong, L. A. van Meeteren, D. A. Egan, M. Sunkara, E. W. van Tilburg, K. Schuurman, O. van Tellingen, A. J. Morris, S. S. Smyth, et al. 2010. Boronic acid-based inhibitor of autotaxin reveals rapid turnover of LPA in the circulation. *Proc. Natl. Acad. Sci. USA* 107: 7257–7262.
35. Stam, J. C., F. Michiels, R. A. van der Kammen, W. H. Moolenaar, and J. G. Collard. 1998. Invasion of T-lymphoma cells: cooperation between Rho family GTPases and lysophospholipid receptor signaling. *EMBO J.* 17: 4066–4074.
36. Krummel, M. F., and I. Macara. 2006. Maintenance and modulation of T cell polarity. *Nat. Immunol.* 7: 1143–1149.
37. Sánchez-Madrid, F., and J. M. Serrador. 2009. Bringing up the rear: defining the roles of the uropod. *Nat. Rev. Mol. Cell Biol.* 10: 353–359.
38. Evans, S. S., W. C. Wang, M. D. Bain, R. Burd, J. R. Ostberg, and E. A. Repasky. 2001. Fever-range hyperthermia dynamically regulates lymphocyte delivery to high endothelial venules. *Blood* 97: 2727–2733.
39. Woolf, E., I. Grigorova, A. Sagiv, V. Grabovsky, S. W. Feigelson, Z. Shulman, T. Hartmann, M. Sixt, J. G. Cyster, and R. Alon. 2007. Lymph node chemokines promote sustained T lymphocyte motility without triggering stable integrin adhesiveness in the absence of shear forces. *Nat. Immunol.* 8: 1076–1085.
40. Zhang, H., X. Xu, J. Gajewiak, R. Tsukahara, Y. Fujiwara, J. Liu, J. I. Fells, D. Perygin, A. L. Parrill, G. Tigyi, and G. D. Prestwich. 2009. Dual activity lysophosphatidic acid receptor pan-antagonist/autotaxin inhibitor reduces breast cancer cell migration in vitro and causes tumor regression in vivo. *Cancer Res.* 69: 5441–5449.
41. Tybulewicz, V. L., and R. B. Henderson. 2009. Rho family GTPases and their regulators in lymphocytes. *Nat. Rev. Immunol.* 9: 630–644.
42. Chettibi, S., A. J. Lawrence, R. D. Stevenson, and J. D. Young. 1994. Effect of lysophosphatidic acid on motility, polarisation and metabolic burst of human neutrophils. *FEMS Immunol. Med. Microbiol.* 8: 271–281.
43. Fulkerson, Z., T. Wu, M. Sunkara, C. V. Kooi, A. J. Morris, and S. S. Smyth. 2011. Binding of autotaxin to integrins localizes lysophosphatidic acid production to platelets and mammalian cells. *J. Biol. Chem.* 286: 34654–34663.
44. Huang, J. H., L. I. Cárdenas-Navia, C. C. Caldwell, T. J. Plumb, C. G. Radu, P. N. Rocha, T. Wilder, J. S. Bromberg, B. N. Cronstein, M. Sitkovsky, et al. 2007. Requirements for T lymphocyte migration in explanted lymph nodes. *J. Immunol.* 178: 7747–7755.
45. Okada, T., and J. G. Cyster. 2007. CC chemokine receptor 7 contributes to Gi-dependent T cell motility in the lymph node. *J. Immunol.* 178: 2973–2978.
46. Worbs, T., T. R. Mempel, J. Bölter, U. H. von Andrian, and R. Förster. 2007. CCR7 ligands stimulate the intranodal motility of T lymphocytes in vivo. *J. Exp. Med.* 204: 489–495.
47. Gérard, A., R. A. van der Kammen, H. Janssen, S. I. Ellenbroek, and J. G. Collard. 2009. The Rac activator Tiam1 controls efficient T-cell trafficking and route of transendothelial migration. *Blood* 113: 6138–6147.
48. Boscacci, R. T., F. Pfeiffer, K. Gollmer, A. I. Sevilla, A. M. Martin, S. F. Soriano, D. Natale, S. Henrickson, U. H. von Andrian, Y. Fukui, et al. 2010. Comprehensive analysis of lymph node stroma-expressed Ig superfamily members reveals redundant and nonredundant roles for ICAM-1, ICAM-2, and VCAM-1 in lymphocyte homing. *Blood* 116: 915–925.
49. Park, E. J., A. Peixoto, Y. Imai, A. Goodarzi, G. Cheng, C. V. Carman, U. H. von Andrian, and M. Shimaoka. 2010. Distinct roles for LFA-1 affinity regulation during T-cell adhesion, diapedesis, and interstitial migration in lymph nodes. *Blood* 115: 1572–1581.
50. Heasman, S. J., L. M. Carlin, S. Cox, T. Ng, and A. J. Ridley. 2010. Coordinated RhoA signaling at the leading edge and uropod is required for T cell transendothelial migration. *J. Cell Biol.* 190: 553–563.
51. Zhao, J., D. He, E. Berdyshev, M. Zhong, R. Salgia, A. J. Morris, S. S. Smyth, V. Natarajan, and Y. Zhao. 2011. Autotaxin induces lung epithelial cell migration through lysoPLD activity-dependent and -independent pathways. *Biochem. J.* 439: 45–55.
52. Hausmann, J., S. Kamtekar, E. Christodoulou, J. E. Day, T. Wu, Z. Fulkerson, H. M. Albers, L. A. van Meeteren, A. J. Houben, L. van Zeijl, et al. 2011. Structural basis of substrate discrimination and integrin binding by autotaxin. *Nat. Struct. Mol. Biol.* 18: 198–204.
53. Nishimasu, H., S. Okudaira, K. Hama, E. Mihara, N. Dohmae, A. Inoue, R. Ishitani, J. Takagi, J. Aoki, and O. Nureki. 2011. Crystal structure of autotaxin and insight into GPCR activation by lipid mediators. *Nat. Struct. Mol. Biol.* 18: 205–212.
54. Goetzl, E. J., and H. Rosen. 2004. Regulation of immunity by lysosphingolipids and their G protein-coupled receptors. *J. Clin. Invest.* 114: 1531–1537.
55. Yanagida, K., K. Masago, H. Nakanishi, Y. Kihara, F. Hamano, Y. Tajima, R. Taguchi, T. Shimizu, and S. Ishii. 2009. Identification and characterization of a novel lysophosphatidic acid receptor, p2y5/LPA6. *J. Biol. Chem.* 284: 17731–17741.
56. Jiang, G., Y. Xu, Y. Fujiwara, T. Tsukahara, R. Tsukahara, J. Gajewiak, G. Tigyi, and G. D. Prestwich. 2007. Alpha-substituted phosphonate analogues of lysophosphatidic acid (LPA) selectively inhibit production and action of LPA. *ChemMedChem* 2: 679–690.
57. Rosen, H., M. G. Sanna, S. M. Cahalan, and P. J. Gonzalez-Cabrera. 2007. Tipping the gatekeeper: S1P regulation of endothelial barrier function. *Trends Immunol.* 28: 102–107.
58. Schwab, S. R., and J. G. Cyster. 2007. Finding a way out: lymphocyte egress from lymphoid organs. *Nat. Immunol.* 8: 1295–1301.